Rupture-dependent breakdown energy in fault models with thermo-hydro-mechanical processes

Valère Lambert[1] and Nadia Lapusta[1,2]

[1]Seismological Laboratory, California Institute of Technology, Pasadena, CA 91125, USA
[2]Department of Mechanical and Civil Engineering, California Institute of Technology, Pasadena, CA 91125, USA
Correspondence: Valère Lambert (vlambert@caltech.edu)

Abstract. Substantial insight into earthquake source processes has resulted from considering frictional ruptures analogous to cohesive-zone shear cracks from fracture mechanics. This analogy holds for slip-weakening representations of fault friction that encapsulate the resistance to rupture propagation in the form of breakdown energy, analogous to fracture energy, prescribed in advance as if it were a material property of the fault interface. Here, we use numerical models of earthquake sequences with enhanced weakening due to thermal pressurization of pore fluids to show how accounting for thermo-hydro-mechanical processes during dynamic shear ruptures makes breakdown energy rupture-dependent. We find that local breakdown energy is neither a constant material property nor uniquely defined by the amount of slip attained during rupture, but depends on how that slip is achieved through the history of slip rate and dynamic stress changes during the rupture process. As a consequence, the frictional breakdown energy of the same location along the fault can vary significantly in different earthquake ruptures that pass through. These results suggest the need for re-examining the assumption of pre-determined frictional breakdown energy common in dynamic rupture modeling and for better understanding of the factors that control rupture dynamics in the presence of thermo-hydro-mechanical processes.

1   Introduction

Fault constitutive relations that describe the evolution of shear resistance with fault motion are critical ingredients of earthquake source modeling. When coupled with the elastodynamic equations of motion, these relations provide insight into the growth and ultimate arrest of ruptures. Earthquake source processes are often considered in the framework of dynamic fracture mechanics, where the earthquake rupture may be considered as a dynamically propagating shear crack (Ida, 1972; Palmer and Rice, 1973; Madariaga, 1976; Kostrov and Das, 1988; Kanamori and Heaton, 2000; Rice, 2000; Kanamori and Brodsky, 2004; Rubin and Ampuero, 2005).

By analogy to cohesive-zone relations for Mode I opening cracks, slip-weakening laws have been commonly used to describe the dynamic decrease in shear resistance during sliding (Ida, 1972; Palmer and Rice, 1973; Madariaga, 1976; Kostrov and Das, 1988; Kanamori and Brodsky, 2004; Bouchon, 1997; Ide and Takeo, 1997; Olsen et al., 1997; Bouchon et al., 1998; Cruz-Atienza et al., 2009; Kaneko et al., 2017; Gallovic et al., 2019). Linear slip weakening is one of the simplest and most

25 commonly used versions, in which the shear resistance decreases linearly with slip from a peak of τ_{peak} to a constant dynamic
level τ_{dyn} achieved at slip of D_c (Fig. 1). The breakdown energy (Fig. 1) is meant to describe the energy next to the rupture
front that controls the rupture dynamics, and is analogous to fracture energy from singular and cohesive zone models of fracture mechanics (Palmer and Rice, 1973; Rice, 1980; Cocco et al., 2004); for the linear slip-weakening friction, it is given by
$G = (\tau_{\text{peak}} - \tau_{\text{dyn}})D_c/2$. The breakdown energy is part of the overall energy partitioning for dynamic ruptures, with the total
30 strain energy change throughout the ruptured region (ΔW) being separated into the radiated energy E_R, breakdown energy G,
and other residual dissipated energy (Kanamori and Rivera, 2006).

More involved fault-constitutive laws are generally required to explain a number of aspects of faulting behavior, most notably the restrengthening of faults in between earthquakes. Laboratory experiments have provided significant insight into the
35 rich behavior of shear resistance, with the frictional response at slip rates between $10^{-9} - 10^{-3}$ m/s being well-described by
rate-and-state friction laws (Dieterich, 2007). A number of previous studies have used models on rate-and-state faults to provide
insight into a number of earthquake and slow slip observations, such as sequences of earthquakes on an actual fault segment
and repeating earthquakes (Chen and Lapusta, 2009; Barbot et al., 2012; Dieterich, 2007, and references therein). While incorporating a more involved dependence of shear resistance on long-term healing, standard Dieterich-Ruina rate-and-state friction
40 has been shown to resemble linear slip-weakening during dynamic rupture (Okubo, 1989; Cocco and Bizzarri, 2002; Lapusta
and Liu, 2009), providing further reinforcement of the notion that the breakdown of shear resistance during dynamic rupture
may be adequately described by slip-weakening behavior.

If slip weakening were the fundamental constitutive behavior describing fault resistance during dynamic rupture, then its
45 parameters - the peak resistance τ_{peak}, dynamic resistance τ_{dyn}, and breakdown energy G - would be expected to be material
properties. Many studies have attempted to infer such fault constitutive properties from the strong-motion data resulting from
natural earthquakes assuming linear slip-weakening behavior (Bouchon, 1997; Ide and Takeo, 1997; Olsen et al., 1997; Bouchon et al., 1998; Cruz-Atienza et al., 2009; Kaneko et al., 2017; Gallovic et al., 2019). Such studies have noted substantial
trade-offs in the constitutive properties during such inversions, such as between the slip-weakening distance D_c and strength
50 excess $\tau_{\text{peak}} - \tau_{\text{ini}}$, where τ_{ini} is the initial stress (Fig. 1). However, it has been presumed that the spatial distribution of static
stress drop and breakdown energy may be the most reliably determined features, as the stress drop can be inferred from the
spatial distribution of slip and remaining variations in rupture speed are largely controlled by the breakdown energy in such linear slip-weakening representations (Guatteri and Spudich, 2000). One of the most notable features of seismologically-inferred
breakdown energies from natural earthquakes is that the average breakdown energy from the rupture process has been inferred
55 to increase with the earthquake size (Abercrombie and Rice, 2005; Rice, 2006; Viesca and Garagash, 2015), which is inconsistent with the breakdown energy being a material property as assumed in linear slip-weakening laws, as well as with nearly
magnitude-independent breakdown energy resulting from standard rate-and-state friction (Perry et al., 2020).

Several theoretical and numerical studies have demonstrated that enhanced dynamic weakening, as widely observed at rel-
60   atively high slip rates ($> 10^3$ m/s) in laboratory experiments (Tullis, 2007; Di Toro et al., 2011), may explain the inferred
increase in breakdown energy with slip (Rice, 2006; Viesca and Garagash, 2015; Perry et al., 2020). A number of different
mechanisms have been proposed for such enhanced weakening, many of them due to shear heating. For example, thermal pres-
surization may occur due to the rapid shear heating of pore fluids during slip (Sibson, 1973; Andrews, 2002; Rice, 2006); if
pore fluids are heated fast enough and not allowed to diffuse away, they pressurize and reduce the effective normal stress on the
65   fault. Flash heating is another thermally-induced weakening mechanism, where the effective friction coefficient is rapidly re-
duced due to local melting of highly stressed micro-contacts along the fault (Rice, 1999; Goldsby and Tullis, 2011; Passelegue
et al., 2014). Considerations of heat production during dynamic shear ruptures provide a substantial constraint for potential
fault models, as field studies show no correlation between faulting and heat flow signatures and rarely suggest the presence
of melt (Sibson, 1975; Lachenbruch and Sass, 1980). Models with enhanced weakening have been successful in producing
70   fault operation at low overall prestress and low heat production (Rice, 2006; Noda et al., 2009; Lambert et al., in review) as
supported by several observations (Brune et al., 1969; Zoback et al., 1987; Hickman and Zoback, 2004; Williams et al., 2004).

Numerical models have shown that the incorporation of thermally-activated enhanced weakening mechanisms during dy-
namic rupture can have profound effects on the evolution of individual ruptures, as well as the long-term behavior of fault
75   segments, with the potential to make seemingly stable creeping regions fail violently during earthquakes (Noda and Lapusta,
2013), and for the deeper penetration of large ruptures, which may explain the seismic-quiescence of mature faults that have
historically hosted large earthquakes (Jiang and Lapusta, 2016). Despite evolving dynamic resistance in such models, they can
also be consistent with magnitude-invariant static stress drops (Perry et al., 2020).

At the same time, accounting for thermo-hydro-mechanical processes during dynamic rupture can clearly weaken or even
80   remove the analogy between frictional shear ruptures and idealized shear cracks of fracture mechanics. The analogy is based
on two key assumptions: 1) that the breakdown of shear resistance is concentrated in a small region near the rupture front,
referred to as small-scale yielding, and 2) that there exists a constant residual stress level $\tau_{\mathrm{dyn}} = \tau_{\mathrm{min}}$ throughout the ruptured
region during sliding (Palmer and Rice, 1973; Freund, 1990). Clearly, these assumptions can become invalid when thermo-
85   hydro-mechanical processes are considered. For example, shear heating can raise the pore fluid pressure in regions away
from the rupture front and weaken the fault there, contributing to the breakdown of fault resistance away from the rupture tip
and varying the dynamic resistance level. Furthermore, the shear heating itself would depend not on the energy counted as
"breakdown" but on the overall dissipated energy, making the fault weakening - and hence rupture dynamics - dependent on
the absolute stress levels, and not just on stress changes, as typically considered by analogy with traditional fracture mechanics.
90

Here, we use numerical models of earthquake sequences with enhanced weakening due to thermal pressurization to illustrate
how the inclusion of thermo-hydro-mechanical processes during dynamic shear ruptures makes breakdown energy rupture-
dependent, in that the value of both local and average breakdown energy vary among ruptures on the same fault with constant

constitutive properties. As such, the breakdown energy is not an intrinsic material property, but takes different values at a given
95   location, depending on the details of the rupture process, which in part depend on the prestress before the dynamic rupture
achieved as a consequence of prior fault slip history. Moreover, the local breakdown energy is not uniquely defined by the
amount of slip attained during rupture, but depends on how that slip was achieved through the complicated history of slip rate
and dynamic stress changes throughout the rupture process.

2   Description of numerical models

100   We conduct numerical simulations of spontaneous sequences of earthquakes and aseismic slip (SEAS) utilizing the spectral
boundary integral method to solve the elastodynamic equations of motion coupled with friction boundary conditions, including
the evolution of pore fluid pressure and temperature on the fault coupled with off-fault diffusion (Lapusta et al., 2000; Noda and
Lapusta, 2010). Our simulations consider mode III slip on a 1-D fault embedded into a 2-D uniform, isotropic, elastic medium
slowly loaded with a long-term slip rate V_{pl} (Fig. 2). The simulations resolve the full slip behavior throughout earthquake
105   sequences, including the nucleation process, the propagation of individual dynamic ruptures, as well as periods of post-seismic
and the interseismic slip between events that can last for months to hundreds of years.

Our fault models adopt the laboratory-derived Dieterich-Ruina rate-and-state friction law with the state evolution governed
by the aging law (Dieterich, 1979; Ruina, 1983):

$$\tau = \overline{\sigma} f(V, \theta) = (\sigma - p) \left[f_* + a \log \frac{V}{V_*} + b \log \frac{\theta V_*}{D_{\mathrm{RS}}} \right], \tag{1}$$

$$\dot{\theta} = 1 - \frac{V\theta}{D_{\mathrm{RS}}}, \tag{2}$$

where $\overline{\sigma}$ is the effective normal stress, σ is the normal stress, p is the pore fluid pressure, f_* is the reference steady-state friction
coefficient at reference sliding rate V_*, D_{RS} is the characteristic slip distance, and a and b are the direct effect and evolution ef-
fect parameters, respectively. Other formulations for the evolution of the state variable exist, such as the slip law (Ruina, 1983)
115   as well as various composite laws, and the formulation that best describes various laboratory experiments remains a topic of
ongoing research (Bhattacharya et al., 2015, 2017; Shreedharan et al., 2019). However, the choice of the state evolution law
should not substantially influence the results of this study, as the evolution of shear resistance during dynamic rupture within
our simulations is dominated by the presence of enhanced weakening mechanisms. We use the version of the expressions (1)
and (2) regularized for zero and negative slip rates (Noda and Lapusta, 2010).

120

During conditions of steady-state sliding ($\dot{\theta} = 0$), the friction coefficient is expressed as:

$$f_{ss}(V) = f_* + (a - b) \log \frac{V}{V_*}. \tag{3}$$

The combination of frictional properties $(a - b) > 0$ results in steady-state velocity-strengthening (VS) behavior, where stable
slip is expected, and properties resulting in $(a - b) < 0$ lead to steady-state velocity-weakening (VW) behavior, where acceler-

125 ating slip and hence stick-slip occur for sufficiently large regions (Rice and Ruina, 1983; Rice et al., 2001; Rubin and Ampuero, 2005).

The total fault domain of size λ is partitioned into a frictional region of size λ_{fr} where we solve for the balance of shear stress and frictional resistance, as well as loading regions at the edges where the fault is prescribed to slip at a tectonic plate rate

130 (Fig. 2A). The frictional interface is composed of a 24-km region with VW frictional properties of size λ_{VW}, surrounded by a velocity-strengthening domain. The majority of the seismic events arrest within the VW region, which we refer to as "partial ruptures," however some span the entire VW region, which we refer to as "complete ruptures" (Fig. 2C).

Laboratory experiments indicate that the standard rate-and-state laws (Eqs. 1 - 2) provide good descriptions of frictional

135 behavior at relatively slow slip rates (10^{-9} to 10^{-3} m/s). However, at higher sliding rates, including average seismic slip rates of $\sim$1 m/s, additional enhanced weakening mechanisms can occur, such as the thermal pressurization or pore fluids. Thermal pressurization is governed in our simulations by the following coupled differential equations for the evolution of temperature and pore fluid pressure (Noda and Lapusta, 2010):

$$\frac{\partial T(y,z;t)}{\partial t} = \alpha_{\text{th}} \frac{\partial^2 T(y,z;t)}{\partial y^2} + \frac{\tau(z;t)V(z;t)}{\rho c} \frac{\exp(-y^2/2w^2)}{\sqrt{2\pi}w}, \tag{4}$$

140
$$\frac{\partial p(y,z;t)}{\partial t} = \alpha_{\text{hy}} \frac{\partial^2 p(y,z;t)}{\partial y^2} + \Lambda \frac{\partial T(y,z;t)}{\partial t}, \tag{5}$$

where T is the pore fluid temperature, α_{th} is the thermal diffusivity, τV is the shear heating source which is distributed over a Gaussian shear layer of half-width w, ρc is the specific heat, y is the fault-normal distance, α_{hy} is the hydraulic diffusivity, and Λ is the coupling coefficient that provides the change in pore pressure per unit temperature change under undrained conditions.

145 The parameter values used for the simulations presented in this work are motivated by prior studies (Rice, 2006; Noda and Lapusta, 2010; Perry et al., 2020) and provided in Table 1.

3 Energy partitioning and notion of breakdown energy G

In the earthquake energy budget, the total strain energy change per unit source area $\Delta W/A$ is partitioned into the dissipated energy per unit area, E_{Diss}/A, and the radiated energy per unit area, E_R/A:

150
$$\Delta W/A = E_{\text{Diss}}/A + E_R/A. \tag{6}$$

The total strain energy released per unit area $\Delta W/A$ is given by:

$$\Delta W/A = \frac{1}{2}(\bar{\tau}_{\text{ini}} + \bar{\tau}_{\text{fin}})\bar{\delta}, \tag{7}$$

where $\bar{\delta}$ is the average final slip for the event, and $\bar{\tau}_{\text{ini}}$ and $\bar{\tau}_{\text{fin}}$ are the average initial and final shear stress weighted by the final slip, respectively,

$$\bar{\tau}_{\text{ini}} = \frac{\int_\Sigma \tau_{\text{ini}}(z)\delta_{\text{fin}}(z)dz}{\int_\Sigma \delta_{\text{fin}}(z)dz},$$
(8)

$$\bar{\tau}_{\text{fin}} = \frac{\int_\Sigma \tau_{\text{fin}}(z)\delta_{\text{fin}}(z)dz}{\int_\Sigma \delta_{\text{fin}}(z)dz}.$$
(9)

The static stress drop is a measure of the difference in average stress before and after the rupture. The relevant definition of average static stress drop for energy considerations is the energy-based or slip-weighted stress drop (Noda et al., 2013):

$$\overline{\Delta\tau} = \bar{\tau}_{\text{ini}} - \bar{\tau}_{\text{fin}} = \frac{\int_\Sigma [\tau_{\text{ini}}(z) - \tau_{\text{fin}}(z)]\,\delta_{\text{fin}}(z)dz}{\int_\Sigma \delta_{\text{fin}}(z)dz}.$$
(10)

The dissipated energy per unit rupture area can be computed from the evolution of shear resistance with slip:

$$E_D/A = \frac{\int_\Omega \left[\int_0^{\delta_{\text{fin}}(z)} \tau(\delta')d\delta'\right] dz}{\int_\Omega dz}.$$
(11)

The dissipated energy E_D/A is often further partitioned into the average breakdown energy G (Palmer and Rice, 1973; Rice, 1980) and residual dissipated energy (dark grey triangle and light grey rectangle in Fig. 1, respectively). The average breakdown energy represents the spatial average of the local breakdown energy G_{loc} within the source region,

$$G = \frac{\int_\Omega G_{\text{loc}}(z)dz}{\int_\Omega dz}$$
(12)

where the local breakdown energy is defined as,

$$G_{\text{loc}}(z) = \int_0^{D_c(z)} [\tau(\delta') - \tau_{\text{min}}(z)]d\delta',$$
(13)

and $\tau_{\text{min}}(z)$ is the minimum local shear resistance during seismic slip after the initial strengthening from the initial to peak shear resistance via the direct effect. D_c is defined as the critical slip distance during the rupture such that $\tau(D_c(z)) = \tau_{\text{min}}(z)$.

Seismological studies have attempted to estimate the average breakdown energy for natural earthquakes based on the standard energy partitioning diagram (Fig. 1) as follows (Abercrombie and Rice, 2005; Rice, 2006):

$$G' = \frac{\bar{\delta}}{2}\left(\overline{\Delta\tau} - \frac{2\mu E_R}{M_0}\right),$$
(14)

where G' is the approximation for the average breakdown energy G, $\bar{\delta}$ is the average slip during the rupture, $\overline{\Delta\tau}$ is the seismologically-inferred average static stress drop, μ is the shear modulus, E_R is the radiated energy and M_0 is the seismic moment. The definition of G' assumes that the rupture area exhibits negligible stress overshoot/undershoot, or that the average

180 level of dynamic resistance during sliding is the same as the final average shear stress. Numerical studies have shown that G' may indeed provide a reasonable estimate of the average breakdown energy (within a factor of 2) for crack-like ruptures, which exhibit mild overshoot/undershoot compared to the static stress drop (Perry et al., 2020), however such estimates can dramatically differ from the true values for ruptures that experience a considerable stress undershoot, as is the case of self-healing pulse-like ruptures (Lambert et al., in review).

4 Breakdown energy in models with thermal pressurization of pore fluids

185 The local slip and stress evolution are determined at every point along the fault within our simulations at all times, thus we can calculate the local dissipation and breakdown energy throughout each rupture as well as study these quantities evolve in different ruptures throughout the sequence. We can also compute the average energy quantities and construct the average stress vs. slip curves for the total rupture process in a manner that preserves the overall energy partitioning (Noda and Lapusta, 2012). We define seismic slip to occur when the local slip velocity exceeds a velocity threshold $V_{\text{thresh}} = 0.01$ m/s. As slip rates during

190 sliding are typically around 1 m/s or higher and drop off rapidly during the arrest of slip, modest changes of this velocity threshold by an order of magnitude produce very mild differences in D_c and G, by less than 1%.

The average breakdown energy G computed from our simulations increase with average slip and matches estimates of breakdown energy for natural events (Fig. 3), as expected from the simplified theoretical considerations (Rice, 2006). As

195 demonstrated in previous numerical studies (Perry et al., 2020), when our fault models combine moderately efficient thermal pressurization with persistently weak conditions, such as from relatively low interseismic effective normal stresses (25 MPa) due to substantial chronic fluid overpressurization, the models produce mostly crack-like ruptures that reproduce all main observations about earthquakes, including magnitude-invariant average static stress drops of 1-10 MPa, breakdown energy values that are quantitatively comparable to estimates from natural earthquakes, and fault temperatures well below representative

200 equilibrium melting temperatures near 1000° C for wet granitic compositions in the shallow crust (Rice, 2006). It is important to note that the presence of enhanced dynamic weakening is critical for producing reasonable values of static stress drop (> 1 MPa) in such fault models with chronic fluid overpressurization; otherwise, the stress changes due to the standard rate-and-state friction would be too low (as they are proportional to the effective normal stress). As such, dynamic weakening due to thermal pressurization still dominates the overall weakening behavior during dynamic rupture. These results suggest that fault models

205 incorporating chronic fault weakness and enhanced weakening may be plausible representations of rupture behavior on mature faults. The work of Perry et al. (2020) and Lambert et al. (in review) provide a broader exploration of models with different parameters, including different levels of interseismic effective stresses and efficiency of enhanced dynamic weakening. Here, we use a representative model to illustrate the resulting properties of the breakdown energy in such models.

210 Let us examine the spatial distribution of shear stress and breakdown energy in three ruptures of varying size within the same simulated sequence of earthquakes (Fig. 4). All three ruptures nucleate, propagate, and arrest predominantly in the VW region

that has uniform fault properties, the only difference being how big the events become. The distribution of shear stress along the fault before each rupture is heterogeneous due to the stress drop from previous ruptures. While each earthquake nucleates in a region with approximately the same locally-high initial stress, the ruptures propagate and arrest over regions with lower

215 prestress. Larger ruptures with more slip experience greater weakening and larger local stress drops in some regions, which facilitates further rupture propagation over areas of lower prestress. As such, while the final average shear stress decreases for larger ruptures, the average initial stress also decreases, resulting in nearly magnitude-invariant average stress drops.

Despite the fault constitutive properties being uniform and constant in time, the breakdown energy varies spatially within

220 each event as well as differs at each location for different ruptures (Figs. 4C and 5). Larger ruptures that experience larger average slip also exhibit more weakening, resulting in the average breakdown energy generally increasing with the rupture size (Fig. 4C). If we examine individual points that are common among all three ruptures, we see that the local breakdown energy also varies as the points experiences different degrees of slip and overall weakening behavior (Fig. 5). This suggests that the local and average breakdown energy is not just a function of the local fault material properties, but a more complicated

225 evolution of effective weakening behavior and stress throughout the rupture.

5   Overall increase of breakdown energy with slip and significant rupture-dependent scatter

Previous theoretical work has demonstrated how the incorporation of thermo-hydro-mechanical processes such as the thermal pressurization of pore fluids can explain the inferred increase in breakdown energy with increasing event size (Rice, 2006). The work of Rice (2006) presented solutions for two end-member cases for the evolution of shear resistance and breakdown

230 energy with thermal pressurization, illustrating how continuous weakening occurs with slip and results in breakdown energy increasing with slip..

If slip occurs within a layer of thickness h that is large enough to justify the neglect of heat and fluid transport, conditions may be considered adiabatic and undrained, which may be relevant for relatively short slip durations (Rice, 2006; Viesca and

235 Garagash, 2015). Under such conditions, the weakening behavior is controlled by the ratio of the coupling coefficient Λ and specific heat ρc, as well as the thickness of the shearing layer h which controls the efficiency of heat production. Assuming a constant friction coefficient f and slip rate V, one can express the evolution of shear resistance τ and breakdown energy G as functions of slip (Rice, 2006),

$$\tau(\delta) = f\left(\sigma - p_0\right)\exp\left(-\frac{f\Lambda}{\rho c}\frac{\delta}{h}\right), \tag{15}$$

240 $$G(\delta) = \frac{\rho c\left(\sigma - p_0\right)h}{\Lambda}\left[1 - \left(1 + \frac{f\Lambda\delta}{\rho ch}\right)\exp\left(-\frac{f\Lambda\delta}{\rho ch}\right)\right]. \tag{16}$$

Under such conditions, increasing slip results in continued weakening of the shear resistance and increasing values of breakdown energy. The continued weakening is the result of shear heating and subsequent pressurization, which remains active as

long as the slip rate and shear stress are non-zero.

245   The inclusion of thermal and hydraulic diffusion introduces a diffusion time-scale to the problem, which governs the efficiency of weakening over extended slip durations. If one considers slip on a mathematical plane, the condition under which diffusive processes are the most efficient, a characteristic weakening time-scale t^*, may be defined assuming a constant friction coefficient and slip rate (Mase and Smith, 1987):

$$t^* = \frac{4}{f^2}\left(\frac{\rho c}{\Lambda}\right)^2 \frac{\left(\sqrt{\alpha_{\text{hy}}} + \sqrt{\alpha_{\text{th}}}\right)^2}{V^2}. \tag{17}$$

250 Rice (2006) demonstrated that this may be related to a characteristic slip-weakening distance for thermal pressurization,

$$L^* = \frac{4}{f^2}\left(\frac{\rho c}{\Lambda}\right)^2 \frac{\left(\sqrt{\alpha_{\text{hy}}} + \sqrt{\alpha_{\text{th}}}\right)^2}{V}, \tag{18}$$

such that the evolution of shear resistance and breakdown energy for slip on a plane may also be expressed as a function of slip (Rice, 2006):

$$\tau(\delta) = f(\sigma - p_0)\exp\left(\frac{\delta}{L^*}\right)\text{erfc}\left(\sqrt{\frac{\delta}{L^*}}\right), \tag{19}$$

255 $$G(\delta) = f(\sigma - p_0)L^*\left[\exp\left(\frac{\delta}{L^*}\right)\text{erfc}\left(\sqrt{\frac{\delta}{L^*}}\right)\left(1 - \frac{\delta}{L^*}\right) - 1 + 2\sqrt{\frac{\delta}{\pi L^*}}\right]. \tag{20}$$

Unlike the case of a critical slip-weakening distance D_c in standard slip-weakening models, the weakening of shear resistance is continuous with increasing slip (Fig. 6a), with L^* providing a measure of how much slip is needed to weaken by a certain degree. Note that the evolution of stress in Eqs. (15) and (19) do not consider the elastic interactions that occur due to non-uniform slip within finite ruptures, and therefore assume that the slip velocity is not only temporally constant, but spatially
260 uniform over the fault.

Both of these thermal pressurization solutions have the convenient feature of expressing the breakdown of shear resistance as a function of slip, drawing familiarity to standard slip-weakening notions of shear fracture. As pointed out by Rice (2006), the representation of breakdown energy purely as a function of slip is a considerable simplification, whereas the physics un-
265 derlying the mechanisms for weakening require that τ is a complicated function of the slip rate history up to the current time. During dynamic rupture, the local slip rate experiences considerable acceleration near the rupture front, resulting in a more pronounced weakening rate (Fig. 6), which in turn facilitates large dynamic stresses and higher slip rates in other parts of the rupture. As the rupture front passes, both the slip rate and weakening rate decrease. However, the slip rate may persists around typical seismic values of 1 m/s until the arrival of arrest waves from the edges of the rupture or local healing. Note that while
270 the slip rates behind the rupture front in our models appear more or less stable around 1 m/s (Fig. 6E and G), they may vary depending on the arrival of wave-mediated dynamic stresses from other slipping regions in the rupture, which drive prolonged slip and therefore modulate the weakening rate due to shear heating mechanisms like thermal pressurization. In general, the

friction coefficient may also vary considerably with the slip rate, particularly when accounting for additional enhanced weakening processes such as flash heating (Rice, 1999; Goldsby and Tullis, 2011; Passelegue et al., 2014).

275

An important consequence of continued fault weakening is that much of the additional dissipated energy, which leads to the increase of breakdown energy with continued slip, is not concentrated near the rupture front (Fig. 6). Moreover, weakening may not actually be strictly monotonic but local points can experience transient increases in shear stress as they begin to arrest, but then are loaded by neighboring slipping regions and forced to slip and weaken further (Fig. 5 and 8). The continued and

280 variable weakening of shear resistance behind the rupture front emphasizes a critical difference between dynamic shear ruptures and mode I fracture, where the crack surface is typically traction-free behind the cohesive zone at the rupture front. The attribution of the continually dissipated energy to the breakdown process governing rupture propagation is also inconsistent with the assumption of small-scale yielding, which facilitated the original mathematical analogy based on laboratory constitutive relations derived at lower slip-rates (Palmer and Rice, 1973).

285

While breakdown energy does not appear to be a constant material property, one may ask if the effects of local weakening due to thermal pressurization may be adequately encapsulated into a slip-weakening formulation such as Eqs. (15-19). To gain insight into such possibility, let us examine three large ruptures in our simulations that have comparable average slip and breakdown energy (Fig. 7). If we consider the evolution of local shear stress and slip at points shared among the three ruptures,

290 we can see that the local breakdown energy differs even for comparable local slip. Moreover, the three points, which share the same constitutive description, do not exhibit a systematic scaling relationship between local slip and breakdown energy. For example, the point at $z = -4.8$ km exhibits a generally increasing trend in local G with increasing slip, whereas the point at $z = 4.8$ km shows decreasing values of G for increasing slip among the three ruptures (Fig. 7C vs. E). The point in the center of the rupture ($z = 0$) does not even exhibit a monotonic trend, as G both increases and decreases for ruptures with increasing

295 slip (Fig. 7D). Indeed, if we examine the spatial distribution of local stress and breakdown energy within each rupture, we see that while the three ruptures have comparable average G and slip, they achieve both in different ways (Fig. 8).

The general trend of increasing breakdown energy with slip qualitatively holds for most local points within our simulated ruptures, however there is considerable variability for individual values of G at a given slip (Fig. 9). While values of average

300 breakdown energy and slip for individual ruptures appear to demonstrate a consistent scaling relationship, these average values smooth out the greater variability in local breakdown energy and slip. For points within our simulated ruptures that experience a net decrease in shear stress, the local G is generally within a factor of 3 of the scaling relationship between average G and average slip. This variation adds up to approximately an order of magnitude variation in local G for some values of slip. For frictional ruptures, substantial slip may occur in regions that experience a net increase in shear stress, particularly in the regions

305 near the rupture's arrest (Fig. 5B). We find that points in our simulated ruptures that experience a net increase in shear stress exhibit greater variability in G with slip (Fig. 9, yellow circles), potentially due to the greater variability in slip rate during

rupture deceleration and arrest.

310   Note that this variability in local G for a given slip is achieved among points with uniform and constant constitutive properties. Such variability in the effective weakening rate and G may become more pronounced in the presence of fault heterogeneity, such as for geometrically rough faults with variable effective normal stress, or if the hydraulic properties of the shearing layer and surrounding rock were to evolve during the rupture process, such as from changes in rock permeability due to off-fault damage. The evolution of permeability during dynamic rupture may have considerable implications for the role of thermo-hydro-mechanical processes in the evolution of shear resistance on faults and it is an important topic for future work.

315

   While we follow the assumption that most of the breakdown energy occurs on the shearing surface (Rice, 2006; Viesca and Garagash, 2015), additional dissipation may also come from the production of damage and off-fault inelastic deformation (Poliakov et al., 2002; Andrews, 2005; Okubo et al., 2019), especially on rough, non-planar faults (Dunham et al., 2011b). Such sources of additional dissipated energy may contribute to the inferred increase in average breakdown energy with average slip
320   for natural earthquakes. Estimates from laboratory and field measurements suggest that the contribution of damage and other off-fault processes to dissipation may be relatively small, <10 % (Chester et al., 2005; Rockwell et al., 2009; Aben et al., 2019), however, this remains an area of active research. Since the off-fault damage would be rupture-dependent as well, adding it to the consideration of the breakdown energy would likely further reinforce the conclusion of this study that breakdown energy is not an intrinsic material property but rather is rupture-dependent.

325   **6   Conclusions**

The average breakdown energy for our simulated ruptures tends to increase with increasing rupture size and average slip in a manner consistent with inferences from field observations and simplified theoretical models (Rice, 2006). At the same time, the values of local breakdown energy for a given amount of slip have a wide spread in our simulations, even though the constitutive properties are uniform and constant along the fault, highlighting the reality that breakdown energy in models with
330   thermo-hydro-mechanical mechanisms is not fundamentally a function of slip. In fact, ruptures with near-uniform slip can have local values of the breakdown energy vary by as much as a factor of 4 (Fig. 8C), making a homogeneous fault appear to be heterogeneous. This is because the breakdown energy depends on the specific history of motion and dynamic stress changes that occur throughout individual rupture processes. Furthermore, since the history of rupture motion is determined, in part, by the fault prestress before the dynamic rupture, the breakdown energy also depends on the history of other slip events on the
335   fault that determine the prestress.

   The analytic formulations for the evolution of shear resistance with slip for the thermal pressurization presented by Rice (2006) provide profound insight into the first-order behavior of such thermally-activated hydro-mechanical weakening mechanisms. However, they are based on the kinematic assumptions of a *spatially uniform and temporally constant* slip velocity,

340   as well as a constant friction coefficient, that allow for the weakening rate to be determined as a function of slip. In the fully dynamic statement of the problem, the evolving and spatially non-uniform slip rate is a key part of the solution which leads to the evolution in the associated shear heating and weakening/strengthening of the fault that depend not only on the amount of slip but also on how that slip is achieved through the complex history of slip velocity.

345   The finding that the breakdown energy - as well as the weakening rate - can vary substantially along a given rupture and among subsequent ruptures, even for comparable values of slip, suggests that caution is needed in using the inferred breakdown energies from natural events for modeling of future earthquake scenarios. While some dynamic rupture simulations account for thermo-hydro-mechanical effects (Andrews, 2002; Bizzarri and Cocco, 2006; Noda et al., 2009; Schmitt et al., 2015), many employ simplified shear resistance evolutions that prescribe the breakdown energy and/or weakening rate directly, as a local

350 fault (material) property (Richards-Dinger and Dieterich, 2012; Shaw et al., 2018; Gallovic et al., 2019; Dalguer et al., 2020). Some studies increasingly incorporate the effects of inelastic off-fault damage (Dunham et al., 2011a, b; Roten et al., 2017; Withers et al., 2018) which should result in qualitatively similar effects on the breakdown energy. Future work is needed to investigate whether and how the complexity of the local weakening/strengthening behavior experienced by the simulated faults with thermo-hydro-mechanical mechanisms can be translated into simulations with more simplified local relations, e.g. slip-

355 dependent, and still result in similar rupture dynamics.

    Furthermore, several features of faulting in the presence of thermo-hydro-mechanical effects call into question the overall analogy with cohesive-zone dynamic fracture theory and hence the significance of the breakdown energy as the quantity that controls rupture dynamics. The analogy between breakdown and fracture energies, and more broadly frictional faulting and

360 shear cracks of traditional fracture mechanics, requires that the breakdown process be confined close to the rupture tip (small-scale yielding) and the dynamic resistance level be constant; under such conditions, the conclusions of dynamic fracture theory apply, including on the significance of breakdown energy (Freund, 1990). However, neither of these assumptions holds for the faults with thermo-hydro-mechanical processes. The weakening - and hence breakdown process - typically continues with ongoing slip at seismic slip rates on such faults, long after the rupture front passes. As a result, the breakdown process is not

365 confined to the rupture tip and the dynamic resistance level is not constant. Moreover, the total dissipated energy - not just the energy included in the notion of breakdown energy - contributes to shear heating and hence fault weakening in thermo-hydro-mechanical fault models, and hence the entire dissipated energy is bound to affect rupture dynamics as well. These considerations emphasize the need for better understanding of rupture dynamics and its controls in the presence of thermo-hydro-mechanical processes and for more systematic incorporation of such processes in earthquake source modeling.

370   *Data availability.*   The data supporting the analysis and conclusions are accessible through the CaltechDATA repository (https://data.caltech.edu/records/1447).
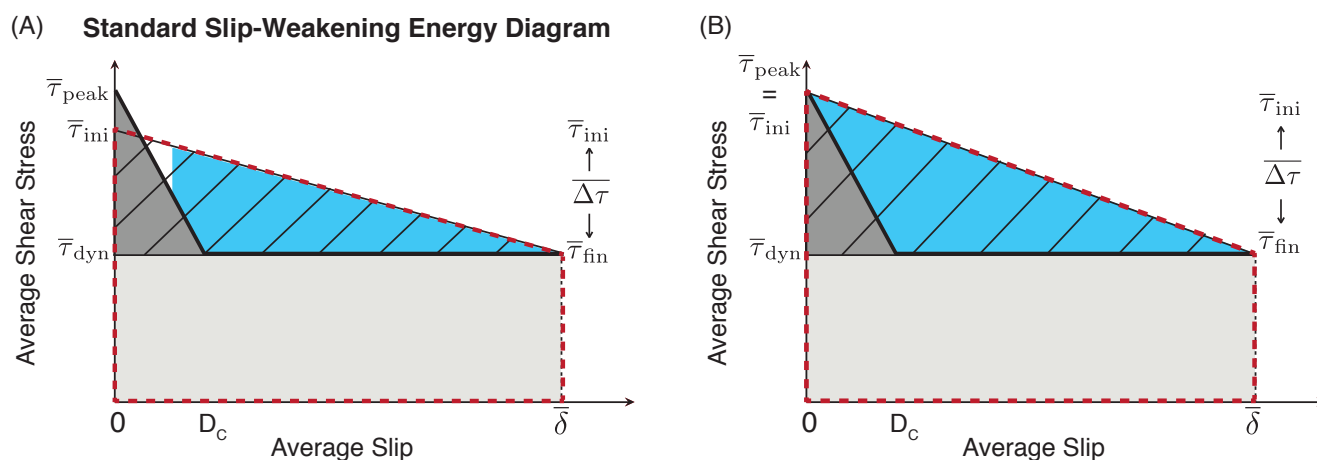
Figure 1. (A) Standard linear slip-weakening diagram where the shear stress is assumed to increase from an initial to peak stress with no slip and then linearly decrease to a dynamic resistance level over a critical slip distance D_c. The difference between the average initial and final shear stress levels is called the static stress drop. The average stress vs. slip diagram is used to represent the energy partitioning of the total strain energy change per unit rupture area (dashed red trapezoid) into the breakdown energy (dark grey triangle), residual dissipated energy per unit area (light gray rectangle), and radiated energy per unit area (blue region). In the case of the initial stress equal to the peak stress, the diagram simplies to that in (B). Note that this diagram is an approximation even if the local behavior is governed by linear slip-weakening friction, since different points of the rupture would have different slip, including near-zero slip close to the rupture edges, and averaging over the dynamic rupture would produce a different curve from the local behavior (Noda and Lapusta, 2012).

Table 1. Model parameters used in simulations of earthquakes and aseismic slip.

Parameter	Symbol	Value
Loading slip rate	V_{pl}	10^{-9} m/s
Shear wave speed	c_s	3299 m/s
Shear modulus	μ	36 GPa
Rate-and-state parameters		
Reference slip velocity	V_*	10^{-6} m/s
Reference friction coefficient	f_*	0.6
Characteristic slip	D_{RS}	1 mm
Rate-and-state direct effect (VW)	a	0.010
Rate-and-state evolution effect (VW)	b	0.015
Rate-and-state direct effect (VS)	a	0.050
Rate-and-state evolution effect (VS)	b	0.003
Thermal pressurization parameters		
Effective normal stress	$\bar{\sigma} = (\sigma - p)$	25 MPa
Coupling coefficient (when TP present)	Λ	0.34 MPa/K
Thermal diffusivity	α_{th}	10^{-6} m^2/s
Hydraulic diffusivity	α_{hy}	10^{-3} m^2/s
Specific heat	ρc	2.7 MPa/K
Shear zone half-width	w	10 mm
Length scales		
Fault length	λ	96 km
Frictional domain	λ_{fr}	72 km
Velocity-weakening region	λ_{VW}	24 km
Cell size	Δx	3.3 m
Quasi-static cohesive zone	Λ_0	75 m
Nucleation size (Rice & Ruina, 1983)	h^*_{RR}	200 m
Nucleation size (Rubin & Ampuero, 2005)	h^*_{RA}	490 m
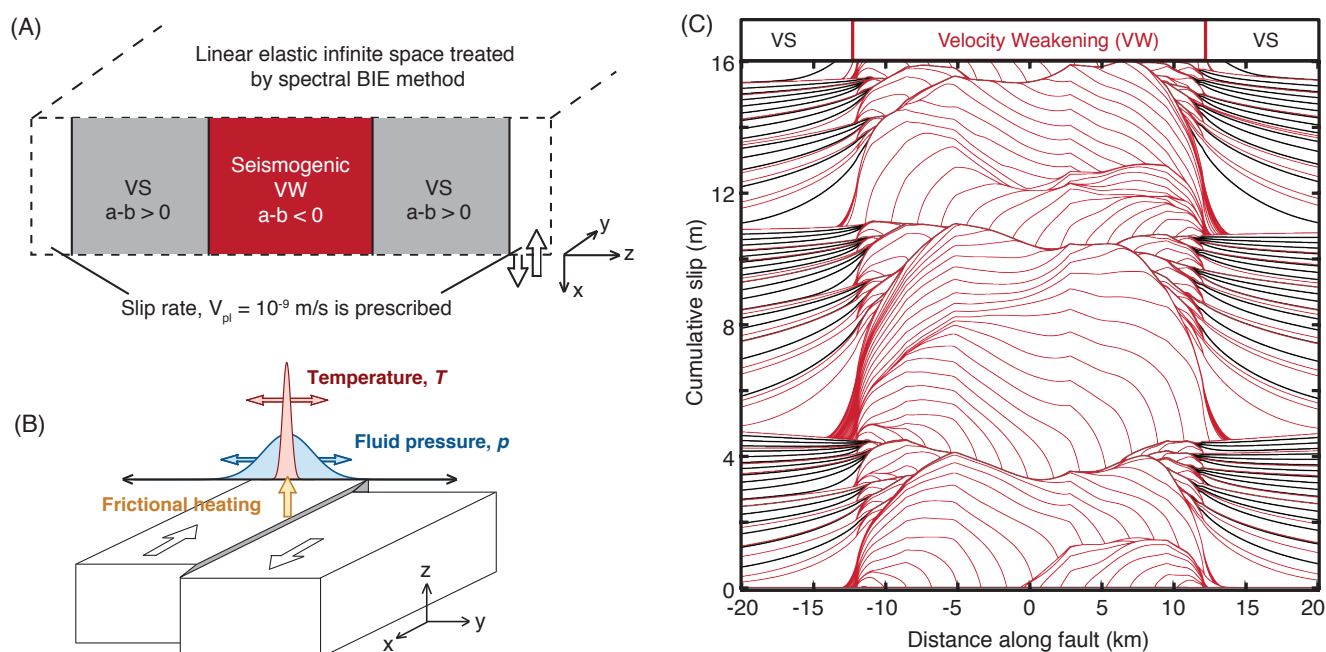
Figure 2. (A) The fault model incorporates a velocity-weakening (VW) seismogenic region surrounded by two velocity-strengthening (VS) sections. A fixed plate rate is prescribed outside of these regions. (B) We incorporate enhanced dynamic weakening due to the thermal pressurization of pore fluids by calculating the evolution of temperature and pore fluid pressure due to shear heating and off-fault diffusion throughout our simulations. (C) The beginning of the accumulated slip history for simulated sequences of crack-like earthquake ruptures and aseismic slip. Seismic events are illustrated in red and plotted every 0.5 seconds while interseismic slip is plotted in black every 10 years. The total simulated slip history spans 2675 years corresponding to cumulative slip of 84 m and contains 200 seismic events.
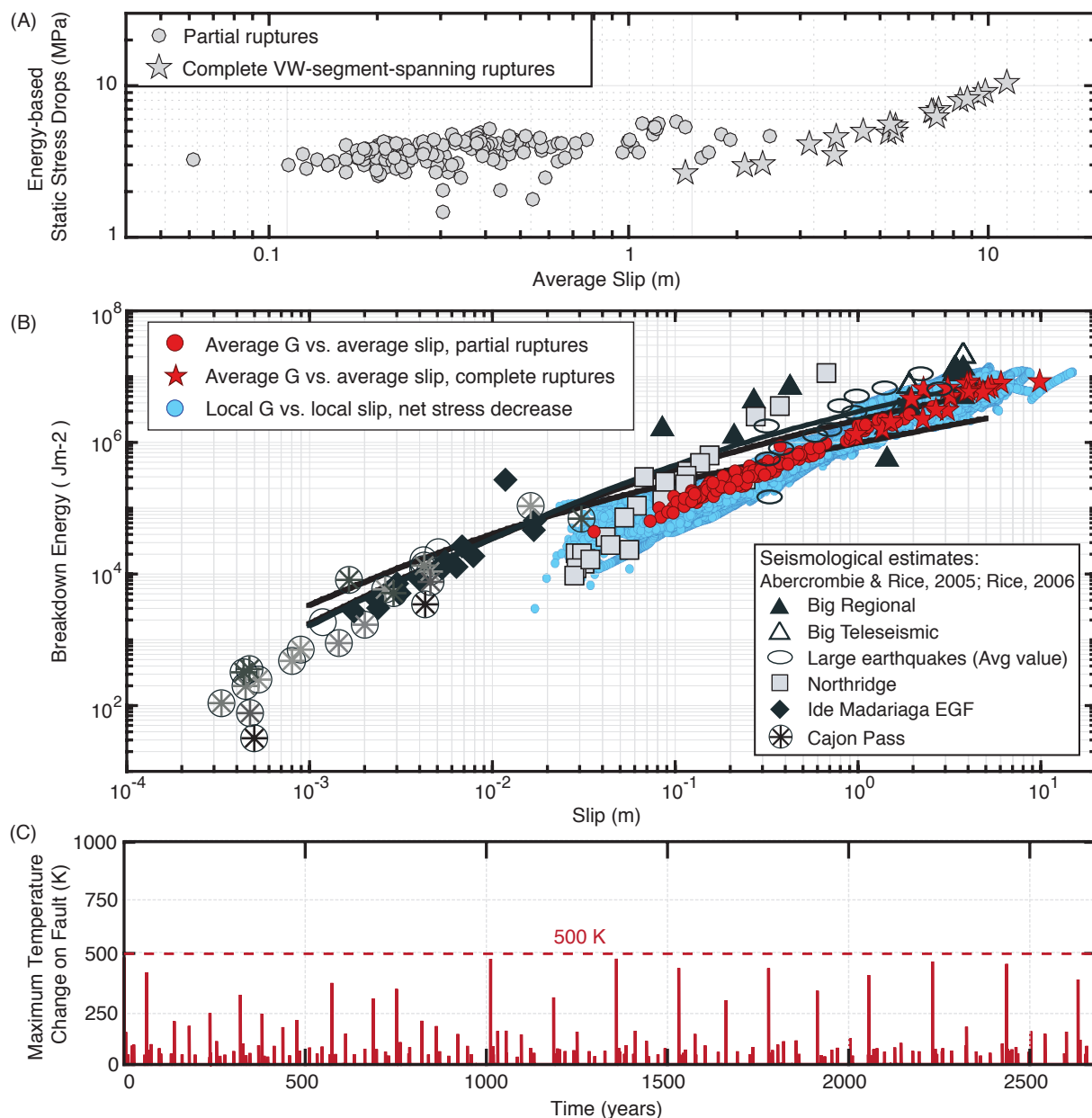
Figure 3. (A) The simulations result in a sequence of mostly crack-like ruptures that, despite including dynamic weakening due to thermal pressurization of pore fluids, are capable of reproducing nearly-magnitude invariant average static stress drops, with values between 1 - 10 MPa. (B) These crack-like ruptures display the overall increasing trend in average breakdown energy with average slip, as inferred for natural earthquakes (Abercrombie and Rice, 2005; Rice, 2006). (C) The simulated fault maintains reasonable temperatures and avoids melting, due to relatively low interseismic effective normal stress of 25 MPa (and hence chronic fluid overpressurization) and sufficiently efficient enhanced weakening due to thermal pressurization of pore fluids.
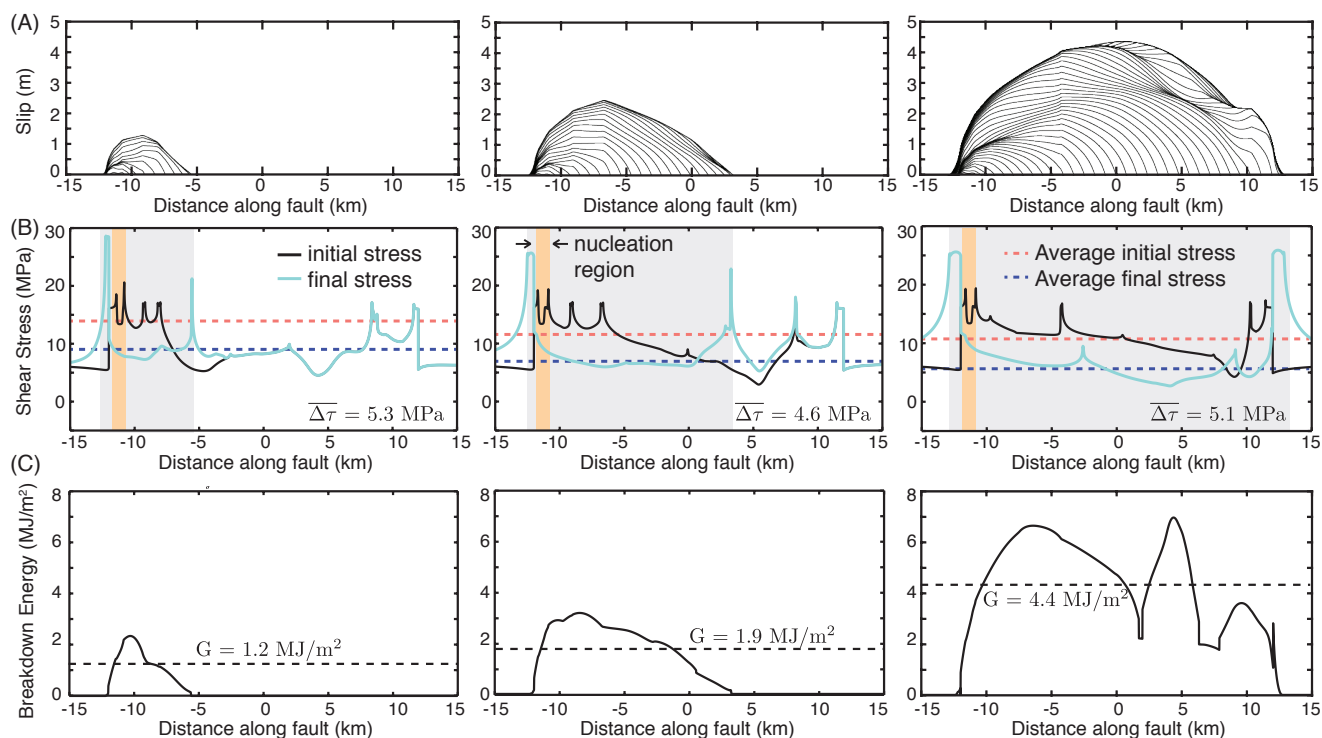
Figure 4. Comparison of three earthquake ruptures of different sizes nucleating over the same fault area. (A) Slip distributions for the three ruptures. (B) Distributions of initial (solid black) and final (solid blue) shear stress for the three ruptures. Gray shading denotes the ruptured region and orange shading denotes the region where each rupture nucleates. The dashed red and blue lines denote the average initial and final shear stress in the ruptured region. Large events have smaller initial and smaller final average stress, resulting in similar stress drops. (C) Distribution of breakdown energy (solid black) and average breakdown energy for each event (dashed line). The average breakdown energy generally increases with the rupture size.
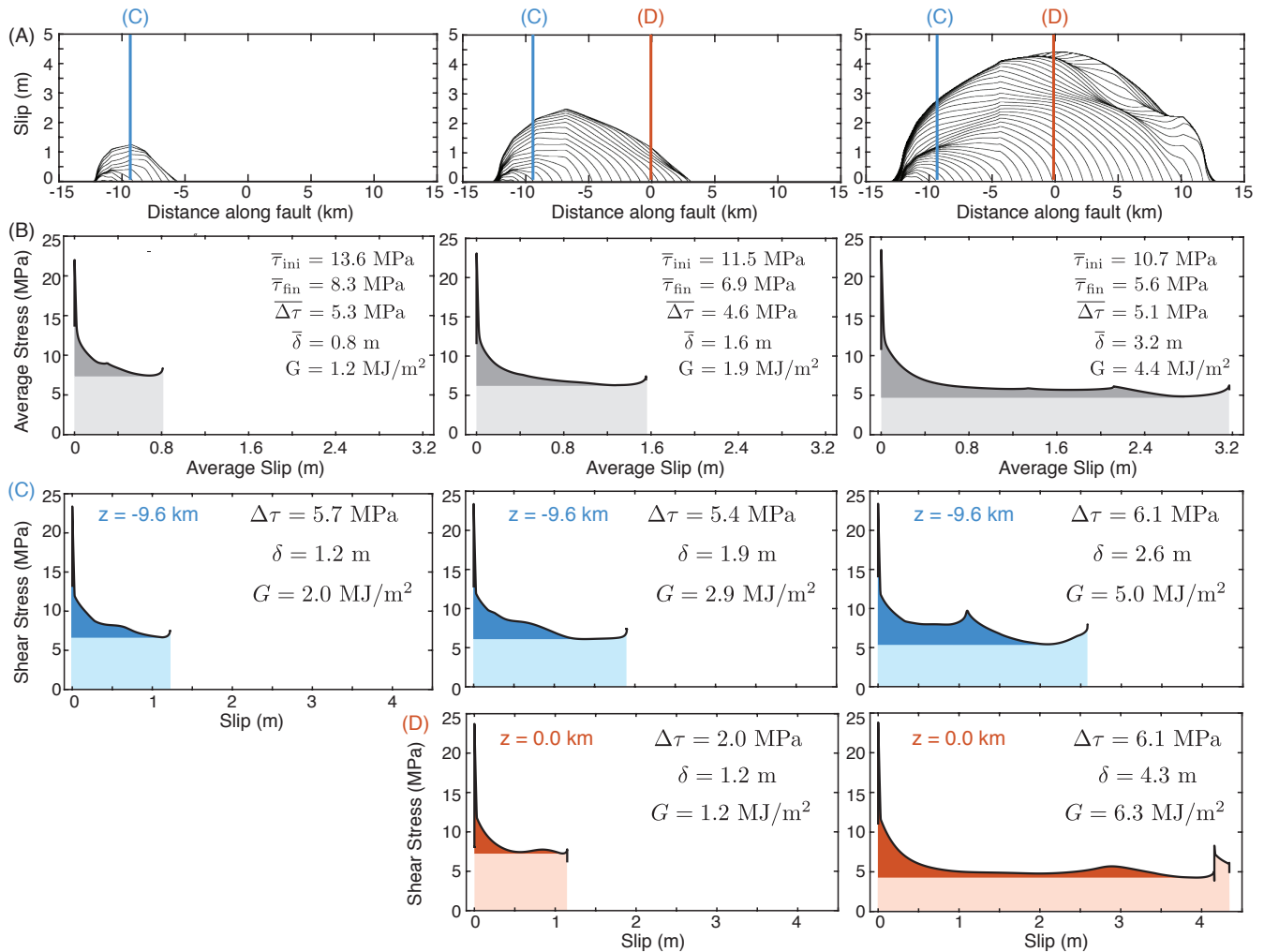
Figure 5. The dependence of shear stress on slip for the three ruptures of Figure 4. A) Slip distributions with locations examined in detail marked. (B) Average shear stress versus slip curves illustrating the energy partitioning of the ruptures, based on the averaging methodology of Noda and Lapusta (2012) that attempts to preserve local rupture behavior. The curves capture the continuous weakening with slip experienced by most rupture locations. (C-D) Local shear stress versus slip curves at two points within the three ruptures, illustrating the general trend in increasing breakdown energy with increasing slip at the same point.
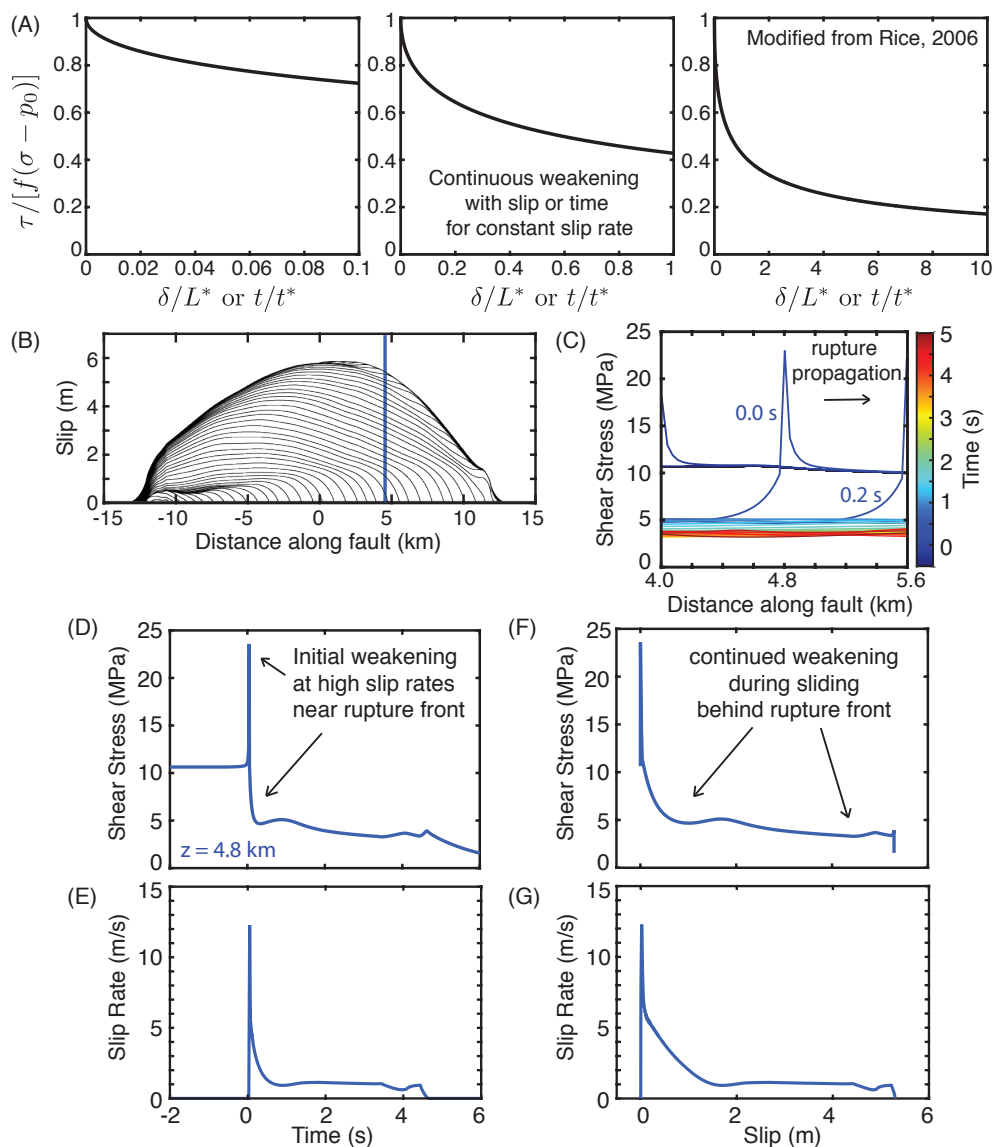
Figure 6. (A) Prediction of continuous weakening of shear resistance with slip or time due to the thermal pressurization of pore fluids during slip on a plane at constant slip rate V and constant friction coefficient f (Rice, 2006). (B) Evolution of slip during a dynamic rupture, slip contoured every 0.2 s. (C) Evolution of shear stress localized around the point $z = 4.8$ km within the rupture. The time window shown corresponds to the duration of sliding at seismic slip rates at $z = 4.8$ m. (D-E) Evolution of local shear stress and slip rate with time at the point indicated by the blue line in (B). (F-G) Evolution of local shear stress and slip rate with slip at the same point. While qualitatively consistent with (A) in terms of the continued weakening with slip and time, the evolution of shear resistance during dynamic ruptures depends on the more complicated history of slip rate, which varies throughout the rupture process. Most of the initial local weakening occurs at slip rates higher than 1 m/s as the rupture front passes by, followed by more gradual weakening behind the rupture front at lower, but still seismic, slip rates.
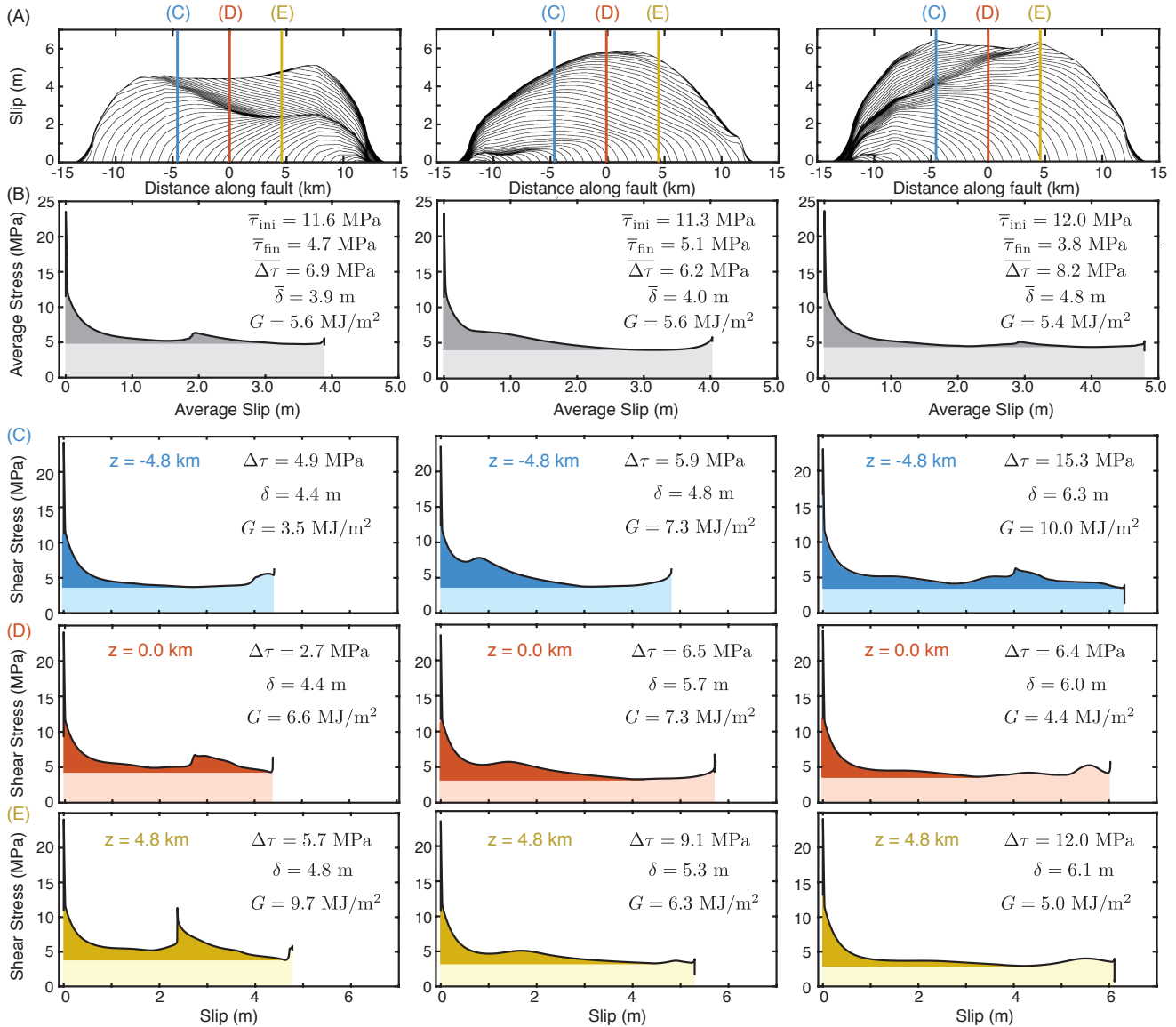
Figure 7. Comparison of local breakdown energy for three large earthquake ruptures with nearly the same average breakdown energy and comparable average slip. (A) Slip distributions for the three ruptures. (B) Average shear stress versus slip curves illustrating the energy partitioning of the ruptures. (C-E) Local shear stress versus slip curves at three points within the ruptures. There is not a strictly increasing trend of breakdown energy with slip for all points. In (C), the point $z = -4.8$ km experiences increasing G with increasing slip. However, in (E), the point $z = 4.8$ km experiences lower values of G in ruptures with larger local slip.
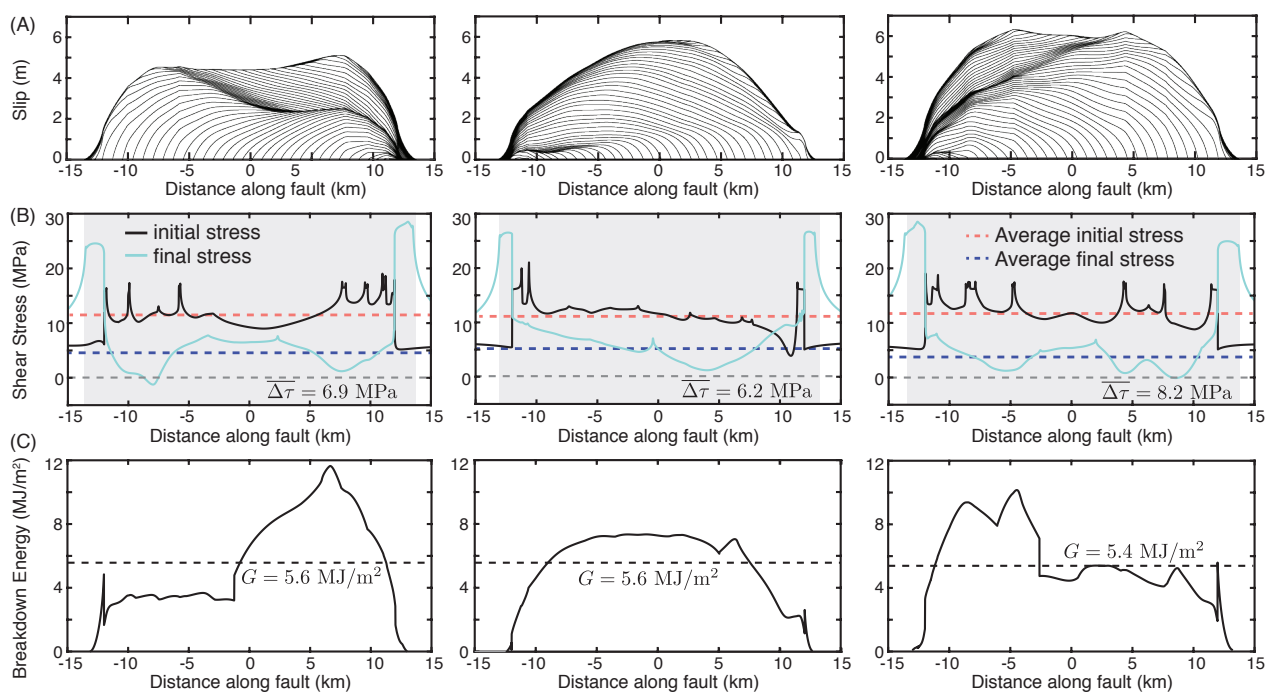
Figure 8. Comparison of the spatial breakdown energy distribution for the three large earthquake ruptures with nearly the same average breakdown energy and comparable average slip of Fig. 7. (A) Slip distributions for the three ruptures. (B) Spatial distributions of initial (solid black) and final (solid blue) shear stress for the three ruptures. Gray shading denotes the ruptured region and dashed red and blue lines indicate the average initial and final shear stresses, respectively. (C) Spatial distributions of the local breakdown energy. While the three ruptures have comparable average breakdown energy, the spatial variation throughout the rupture process considerably differs. Furthermore, the same spatial locations can have significantly different breakdown energy values in different rupture events of comparable size.
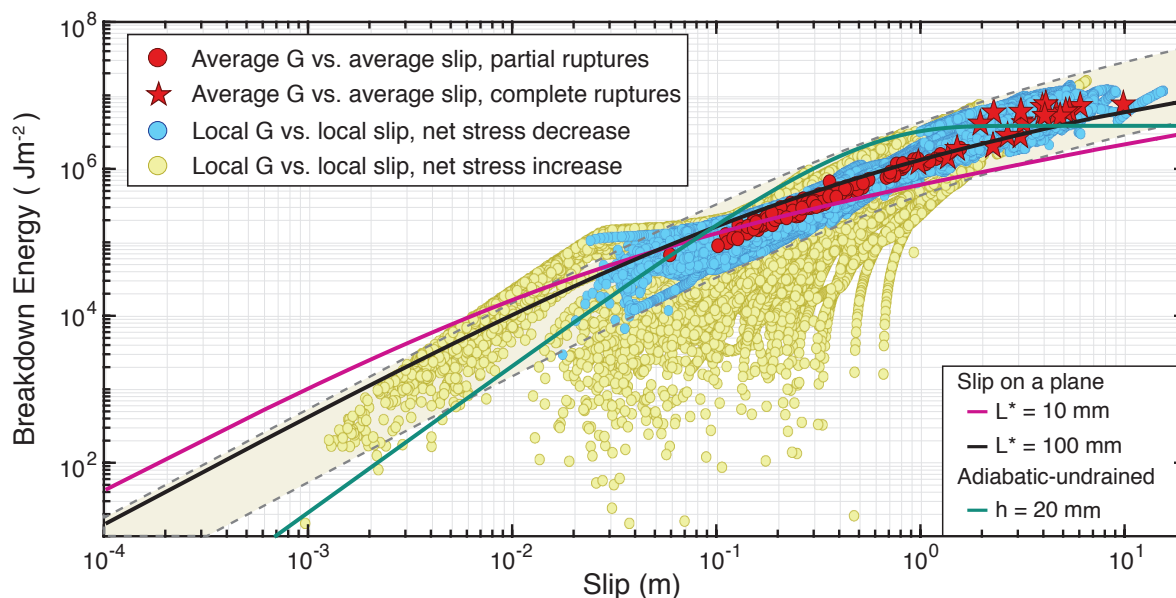
Figure 9. The average and local breakdown energy values for the simulated ruptures show an increasing trend with average and local slip, consistent with inferences from natural earthquakes (Fig. 3). The general trend of increasing breakdown energy with slip qualitatively holds for local points within our simulated ruptures; however, there is considerable variability for individual values of G at a given slip. For points that exhibit net weakening behavior in our simulated ruptures (blue circles), local values of G tend to vary within a factor of 3 from the scaling relationship between average G and average slip. The shaded band bordered by grey dashed lines illustrates the variation in G at a given value of slip. Local values of G are more variable for regions that experience a net increase in stress during the rupture process (yellow circles), e.g., regions close to rupture arrest. Solid lines indicate theoretical curves for G vs. slip based on Eqs. (15) and (19), with the coefficient of friction of $f = 0.53$ and values otherwise indicated in Table 1.

Author contributions. V.L. and N.L. both contributed to developing the main ideas, designing the modeling, and producing the manuscript. V.L. carried out and analyzed the presented numerical experiments.

Competing interests. The authors declare no competing financial interests.

375 *Acknowledgements.* This study was supported by the National Science Foundation (grant EAR 1724686), the United States Geological Survey (grant G19AP00059), and the Southern California Earthquake Center (SCEC), contribution No. 19085. SCEC is funded by NSF Cooperative Agreement EAR-1033462 and USGS Cooperative Agreement G12AC20038. Numerical simulations for this study were carried out on the High Performance Computing Center cluster of the California Institute of Technology.

References

380 Aben, F. M., Brantut, N., Mitchell, T. M., and David, E. C.: Rupture Energetics in Crustal Rock From Laboratory-Scale Seismic Tomography,
Geophysical Research Letters, 46, 7337–7344, https://doi.org/10.1029/2019GL083040, 2019.

Abercrombie, R. E. and Rice, J. R.: Can observations of earthquake scaling constrain slip weakening?, Geophysical Journal International,
162, 406–424, https://doi.org/10.1111/j.1365-246X.2005.02579.x, 2005.

Andrews, D.: A fault constitutive relation accounting for thermal pressurization of pore fluid, Journal of Geophysical Research: Solid Earth,
385 107, 2002.

Andrews, D. J.: Rupture dynamics with energy loss outside the slip zone, Journal of Geophysical Research, 110,
https://doi.org/10.1029/2004JB003191, 2005.

Barbot, S., Lapusta, N., and Avouac, J.-P.: Under the hood of the earthquake machine: Toward predictive modeling of the seismic cycle,
Science, 336, 707–710, 2012.

390 Bhattacharya, P., Rubin, A. M., Bayart, E., Savage, H. M., and Marone, C.: Critical evaluation of state evolution laws in rate and state friction:
Fitting large velocity steps in simulated fault gouge with time-, slip-, and stress-dependent constitutive laws, Journal of Geophysical
Research: Solid Earth, 120, 6365–6385, https://doi.org/10.1002/2015JB012437, 2015.

Bhattacharya, P., Rubin, A. M., and Beeler, N. M.: Does fault strengthening in laboratory rock friction experiments really depend primarily
upon time and not slip?, Journal of Geophysical Research: Solid Earth, 122, 6389–6430, https://doi.org/10.1002/2017JB013936, 2017.

395 Bizzarri, A. and Cocco, M.: A thermal pressurization model for the spontaneous dynamic rupture propagation on a three-dimensional fault:
1. Methodological approach, Journal of Geophysical Research: Solid Earth, 111, https://doi.org/10.1029/2005JB003862, 2006.

Bouchon, M.: The state of stress on some faults of the San Andreas System as inferred from near-field strong motion data, Journal of
Geophysical Research: Solid Earth, 102, 11 731–11 744, https://doi.org/10.1029/97JB00623, 1997.

Bouchon, M., Sekiguchi, H., Irikura, K., and Iwata, T.: Some characteristics of the stress field of the 1995 Hyogo-ken Nanbu (Kobe) earth-
400 quake, Journal of Geophysical Research: Solid Earth, 103, 24 271–24 282, https://doi.org/10.1029/98JB02136, 1998.

Brune, J. N., Henyey, T. L., and Roy, R. F.: Heat flow, stress, and rate of slip along the San Andreas fault, California, Journal of Geophysical
Research, 74, 3821–3827, 1969.

Chen, T. and Lapusta, N.: Scaling of small repeating earthquakes explained by interaction of seismic and aseismic slip in a rate and state
fault model, Journal of Geophysical Research, 114, https://doi.org/10.1029/2008JB005749, 2009.

405 Chester, J. S., Chester, F. M., and Kronenberg, A. K.: Fracture surface energy of the Punchbowl fault, San Andreas system, Nature, 437, 133,
2005.

Cocco, M. and Bizzarri, A.: On the slip-weakening behavior of rate- and state dependent constitutive laws, Geophysical Research Letters,
29, https://doi.org/10.1029/2001GL013999, 2002.

Cocco, M., Bizzarri, A., and Tinti, E.: Physical interpretation of the breakdown process using a rate-and state-dependent friction law, Tectono-
410 physics, 378, 241–262, 2004.

Cruz-Atienza, V. M., Olsen, K. B., and Dalguer, L. A.: Estimation of the Breakdown Slip from Strong-Motion Seismograms: Insights from
Numerical Experiments, Bulletin of the Seismological Society of America, 99, 3454–3469, https://doi.org/10.1785/0120080330, 2009.

Dalguer, L. A., Wu, H., Matsumoto, Y., Irikura, K., Takahama, T., and Tonagi, M.: Development of Dynamic Asperity Models to Predict
Surface Fault Displacement Caused by Earthquakes, Pure and Applied Geophysics, 177, 1983–2006, https://doi.org/10.1007/s00024-019-
415 02255-8, https://doi.org/10.1007/s00024-019-02255-8, 2020.

Di Toro, G., Han, R., Hirose, T., De Paola, N., Nielsen, S., Mizoguchi, K., Ferri, F., Cocco, M., and Shimamoto, T.: Fault lubrication during earthquakes, Nature, 471, 494, 2011.

Dieterich, J.: A constitutive law for rate of earthquake production and its application to earthquake clustering, Journal of Geophysical Research: Solid Earth, 99, 2601–2618, 1994.

420   Dieterich, J.: Applications of Rate- and State-Dependent Friction to Models of Fault Slip and Earthquake Occurrence, in: Treatise on Geophysics, edited by Schubert, G., pp. 107 – 129, Elsevier, Amsterdam, https://doi.org/https://doi.org/10.1016/B978-044452748-6.00065-1, 2007.

Dieterich, J. H.: Modeling of Rock Friction 1. Experimental Results and Constitutive Equations, Journal of Geophysical Research, 84, 2161–2168, 1979.

425   Dunham, E. M., Belanger, D., Cong, L., and Kozdon, J. E.: Earthquake Ruptures with Strongly Rate-Weakening Friction and Off-Fault Plasticity, Partă1: Planar Faults, Bulletin of the Seismological Society of America, 101, 2296–2307, https://doi.org/10.1785/0120100075, 2011a.

Dunham, E. M., Belanger, D., Cong, L., and Kozdon, J. E.: Earthquake Ruptures with Strongly Rate-Weakening Friction and Off-Fault Plasticity, Part 2: Nonplanar Faults, The Bulletin of the Seismological Society of America, 101, 2308–2322,
430   https://doi.org/10.1785/0120100076, 2011b.

Freund, L. B.: Dynamic Fracture Mechanics, Cambridge Monographs on Mechanics, Cambridge University Press, https://doi.org/10.1017/CBO9780511546761, 1990.

Gallovic, F., Valentova, L., Ampuero, J.-P., and Gabriel, A.-A.: Bayesian Dynamic Finite-Fault Inversion: 2. Application to the 2016 Mw 6.2 Amatrice, Italy, Earthquake, Journal of Geophysical Research: Solid Earth, 124, 6970–6988, https://doi.org/10.1029/2019JB017512,
435   2019.

Goldsby, D. L. and Tullis, T. E.: Flash Heating Leads to Low Frictional Strength of Crustal Rocks at Earthquake Slip Rates, Science, 334, 216–218, https://doi.org/10.1126/science.1207902, 2011.

Guatteri, M. and Spudich, P.: What Can Strong-Motion Data Tell Us about Slip-Weakening Fault-Friction Laws?, Bulletin of the Seismological Society of America, 90, 98–116, https://doi.org/10.1785/0119990053, 2000.

440   Hickman, S. and Zoback, M.: Stress orientations and magnitudes in the SAFOD pilot hole, Geophysical Research Letters, 31, 2004.

Ida, Y.: Cohesive force across the tip of a longitudinal-shear crack and Griffith's specific surface energy, Journal of Geophysical Research, 77, 3796–3805, 1972.

Ide, S. and Takeo, M.: Determination of constitutive relations of fault slip based on seismic wave analysis, Journal of Geophysical Research: Solid Earth, 102, 27 379–27 391, https://doi.org/10.1029/97JB02675, 1997.

445   Jiang, J. and Lapusta, N.: Deeper penetration of large earthquakes on seismically quiescent faults, Science, 352, 1293–1297, https://doi.org/10.1126/science.aaf1496, 2016.

Kanamori, H. and Brodsky, E. E.: The Physics of Earthquakes, Reports on Progress in Physics, 67, 1429–1496, https://doi.org/10.1088/0034-4885/67/8/R03, 2004.

Kanamori, H. and Heaton, T. H.: Microscopic and macroscopic physics of earthquakes, Geocomplexity and the Physics of Earthquakes, pp.
450   147–163, 2000.

Kanamori, H. and Rivera, L.: Energy Partitioning during an earthquake, Earthquakes: Radiated energy and the physics of faulting, pp. 3–13, 2006.

Kaneko, Y., Fukuyama, E., and Hamling, I. J.: Slip-weakening distance and energy budget inferred from near-fault ground deformation during the 2016 Mw 7.8 Kaikura earthquake, Geophysical Research Letters, 44, 4765–4773, https://doi.org/10.1002/2017GL073681, 2017.

455 Kostrov, B. V. and Das, S.: Principles of earthquake source mechanics, Cambridge, England ; New York : Cambridge University Press, 1988.

Lachenbruch, A. H. and Sass, J. H.: Heat flow and energetics of the San Andreas Fault Zone, Journal of Geophysical Research: Solid Earth, 85, 6185–6222, https://doi.org/10.1029/JB085iB11p06185, 1980.

Lambert, V., Lapusta, N., and Perry, S.: Do large earthquakes propagate as self-healing pulses or mild cracks?, Nature, in review.

Lapusta, N. and Liu, Y.: Three-dimensional boundary integral modeling of spontaneous earthquake sequences and aseismic slip, Journal of
460 Geophysical Research, 114, B09 303, https://doi.org/10.1029/2008JB005934, 2009.

Lapusta, N., Rice, J. R., Ben-Zion, Y., and Zheng, G.: Elastodynamic Analysis for Slow Tectonic Loading with Sponta- neous Rupture Episodes on Faults with Rate- and State- dependent Friction, Journal of Geophysical Research, 105, 765–789, https://doi.org/10.1029/2000JB900250, 2000.

Madariaga, R.: Dynamics of an Expanding Circular Fault, Bulletin of the Seismological Society of America, 66, 639–666, 1976.

465 Mase, C. W. and Smith, L.: The role of pore fluids in tectonic processes, Reviews of Geophysics, 25, 1348–1358, https://doi.org/10.1029/RG025i006p01348, 1987.

Noda, H. and Lapusta, N.: Three-dimensional earthquake sequence simulations with evolving temperature and pore pres- sure due to shear heating: Effect of heterogeneous hydraulic diffusivity, Journal of Geophysical Research, 115, B123 414, https://doi.org/10.1029/2010JB007780, 2010.

470 Noda, H. and Lapusta, N.: On Averaging Interface Response During Dynamic Rupture and Energy Partitioning Diagrams for Earthquakes, Journal of Applied Mechanics, 79, https://doi.org/10.1115/1.4005964, 2012.

Noda, H. and Lapusta, N.: Stable creeping fault segments can become destructive as a result of dynamic weakening, Nature, 493, 518 EP –, 2013.

Noda, H., Dunham, E. M., and Rice, J. R.: Earthquake ruptures with thermal weakening and the operation of major faults at low overall stress
475 levels, Journal of Geophysical Research: Solid Earth, 114, https://doi.org/10.1029/2008JB006143, 2009.

Noda, H., Lapusta, N., and Kanamori, H.: Comparison of average stress drop measures for ruptures with heterogeneous stress change and implications for earthquake physics, Geophysical Journal International, https://doi.org/10.1093/gji/ggt074, 2013.

Okubo, K., Bhat, H. S., Rougier, E., Marty, S., Schubnel, A., Lei, Z., Knight, E. E., and Klinger, Y.: Dynamics, Radiation, and Overall Energy Budget of Earthquake Rupture With Coseismic Off-Fault Damage, Journal of Geophysical Research: Solid Earth, 124, 11 771–11 801,
480 https://doi.org/10.1029/2019JB017304, 2019.

Okubo, P. G.: Dynamic rupture modeling with laboratory-derived constitutive relations, Journal of Geophysical Research: Solid Earth, 94, 12 321–12 335, https://doi.org/10.1029/JB094iB09p12321, 1989.

Olsen, K. B., Madariaga, R., and Archuleta, R. J.: Three-Dimensional Dynamic Simulation of the 1992 Landers Earthquake, Science, 278, 834–838, https://doi.org/10.1126/science.278.5339.834, 1997.

485 Palmer, A. C. and Rice, J.: The growth of slip surfaces in the progressive failure of over-consolidated clay, Proceedings of the Royal Society of London A: Mathematical, Physical and Engineering Sciences, 332, 527–548, 1973.

Passelegue, F. X., Goldsby, D. L., and Fabbri, O.: The influence of ambient fault temperature on flash-heating phenomena, Geophysical Research Letters, 41, 828–835, https://doi.org/10.1002/2013GL058374, 2014.

Perry, S. M., Lambert, V., and Lapusta, N.: Nearly magnitude-invariant stress drops in simulated crack-like earthquake sequences on rate-and-state faults with thermal pressurization of pore fluids, Journal of Geophysical Research: Solid Earth, 125, e2019JB018 597, https://doi.org/10.1029/2019JB018597, 2020.

Poliakov, A. N. B., Dmowska, R., and Rice, J. R.: Dynamic shear rupture interactions with fault bends and off-axis secondary faulting, Journal of Geophysical Research: Solid Earth, 107, ESE 6–1–ESE 6–18, https://doi.org/10.1029/2001JB000572, 2002.

Rice, J.: Flash heating at asperity contacts and rate-dependent friction, Eos Trans. AGU, 80, F471, 1999.

Rice, J.: Fracture energy of earthquakes and slip-weakening rupture parameters, EOS, Trans. Am. geophys. Un., Fall Meeting Suppl, 81, F1227, 2000.

Rice, J. and Ruina, A. L.: Stability of steady frictional slipping, Journal of Applied Mechanics, 50, 343–349, 1983.

Rice, J. R.: The Mechanics of Earthquake Rupture, in Physics of Earth's Interior, pp. 555–649, 1980.

Rice, J. R.: Heating and weakening of faults during earthquake slip, Journal of Geophysical Research, 111, B05 311, https://doi.org/10.1029/2005JB004006, 2006.

Rice, J. R., Lapusta, N., and Ranjith, K.: Rate and state dependent friction and the stability of sliding between elastically deformable solids, Journal of the Mechanics and Physics of Solids, 49, 1865–1898, 2001.

Richards-Dinger, K. and Dieterich, J. H.: RSQSim Earthquake Simulator, Seismological Research Letters, 83, 983–990, https://doi.org/10.1785/0220120105, 2012.

Rockwell, T., Sisk, M., Girty, G., Dor, O., Wechsler, N., and Ben-Zion, Y.: Chemical and Physical Characteristics of Pulverized Tejon Lookout Granite Adjacent to the San Andreas and Garlock Faults: Implications for Earthquake Physics, Pure and Applied Geophysics, 166, 1725–1746, https://doi.org/10.1007/s00024-009-0514-1, 2009.

Roten, D., Olsen, K. B., and Day, S. M.: Off-fault deformations and shallow slip deficit from dynamic rupture simulations with fault zone plasticity, Geophysical Research Letters, 44, 7733–7742, https://doi.org/10.1002/2017GL074323, 2017.

Rubin, A. and Ampuero, J.-P.: Earthquake nucleation on (aging) rate and state faults, Journal of Geophysical Research: Solid Earth, 110, 2005.

Ruina, A.: Slip Instability and State Variable Friction Laws, Journal of Geophysical Research, 88, 10 359–10 370, 1983.

Schmitt, S. V., Segall, P., and Dunham, E. M.: Nucleation and dynamic rupture on weakly stressed faults sustained by thermal pressurization, Journal of Geophysical Research: Solid Earth, 120, 7606–7640, https://doi.org/10.1002/2015JB012322, 2015.

Shaw, B. E., Milner, K. R., Field, E. H., Richards-Dinger, K., Gilchrist, J. J., Dieterich, J. H., and Jordan, T. H.: A physics-based earthquake simulator replicates seismic hazard statistics across California, Science Advances, 4, https://doi.org/10.1126/sciadv.aau0688, 2018.

Shreedharan, S., Riviere, J., Bhattacharya, P., and Marone, C.: Frictional State Evolution During Normal Stress Perturbations Probed With Ultrasonic Waves, Journal of Geophysical Research: Solid Earth, 124, 5469–5491, https://doi.org/10.1029/2018JB016885, 2019.

Sibson, R. H.: Interactions between temperature and pore-fluid pressure during earthquake faulting and a mechanism for partial or total stress relief., Nature, 243, 66–68, 1973.

Sibson, R. H.: Generation of Pseudotachylyte by Ancient Seismic Faulting, Geophysical Journal of the Royal Astronomical Society, 43, 775–794, https://doi.org/10.1111/j.1365-246X.1975.tb06195.x, 1975.

Tullis, T.: Friction of Rock at Earthquake Slip Rates, Treatise on Geophysics, 4, 131–152, https://doi.org/10.1016/B978-044452748-6.00064-X, 2007.

Viesca, R. C. and Garagash, D. I.: Ubiquitous weakening of faults due to thermal pressurization, Nature Geoscience, 8, 875–879, https://doi.org/10.1038/NGEO2554, 2015.

Williams, C. F., Grubb, F. V., and Galanis, S. P.: Heat flow in the SAFOD pilot hole and implications for the strength of the San Andreas Fault, Geophysical Research Letters, 31, 2004.

Withers, K. B., Olsen, K. B., Day, S. M., and Shi, Z.: Ground Motion and Intraevent Variability from 3D Deterministic Broad-band (0-7.5 Hz) Simulations along a Nonplanar Strike-Slip Fault, Bulletin of the Seismological Society of America, 109, 229–250, https://doi.org/10.1785/0120180006, https://doi.org/10.1785/0120180006, 2018.

Zoback, M. D., Zoback, M. L., Mount, V. S., Suppe, J., Eaton, J. P., Healy, J. H., Oppenheimer, D., Reasenberg, P., Jones, L., Raleigh, C. B., Wong, I. G., Scotti, O., and Wentworth, C.: New Evidence on the State of Stress of the San Andreas Fault System, Science, 238, 1105–1111, https://doi.org/10.1126/science.238.4830.1105, 1987.